A LIGHT-SCATTERING CHARACTERIZATION OF MEMBRANE VESICLES

J. C. SELSER, Y. YEH, *and* R. J. BASKIN

From the Department of Applied Science and Department of Zoology, University of California, Davis, California 95616

ABSTRACT A technique has been developed in this paper which enables quasi-elastic laser light scattering to be used to accurately and quantitatively measure the average vesicle diffusion coefficient and the relative dispersion in the diffusion coefficient about this average for dilute polydisperse vesicle suspensions. This technique relies on a theoretical analysis of a modified form of the Z-averaged diffusion coefficient. This modified Z-averaged diffusion coefficient explicitly incorporates vesicle size, structure, and polydispersity in a description of the scattered light autocorrelation spectrum. Light-scattering experiments were performed on a dilute, lobster sarcoplasmic reticulum vesicle suspension and the measured average diffusion coefficient and the diffusion coefficient relative dispersion about this average were determined with accuracies of 2 and 10%, respectively. A comparison of vesicle size inferred from light-scattering results was made with size results from electron microscopic analysis of the same sample.

INTRODUCTION

It is well-known that membrane fragments extracted from various cellular locations generally form spherical vesicles in solution. The size, molecular structure, and homogeneity of these membrane vesicles are currently of great interest since they often retain their enzymatic activities as well as their ability to transport ions.

Vesicles obtained from sarcoplasmic reticulum (SR) membranes are a particularly suitable system for study due to their ready availability and their relatively simple composition. These vesicles contain one transport enzyme, a calcium transport ATPase. Previous studies (1, 2) have shown that vesicles obtained from lobster muscle are ideally suited for study because of their homogeneity and high rate of calcium transport.

Electron microscopic (EM) studies of lobster SR vesicle preparations show these vesicles to be distributed in size with a typical average radius of 1,000 Å and corresponding shell thickness of 80 Å. From a light-scattering point of view, such suspensions constitute polydisperse systems of large spherical shell scatterers. The vesicle thickness is small enough compared with the wavelength of light in the suspension (about 4,000 Å) to consider these shells as strictly surface distributions of scattering material. In addition, based on the fact that we were not able to detect depolarization of the scattered light from dilute lobster SR suspensions, we concluded that in our

experiments such vesicles could be considered to be of uniform and isotropic composition.

Quasi-elastic laser light scattering (QELS) has been used for about a decade to measure the average diffusion coefficient and the associated hydrodynamic radius of monodisperse suspensions of small macromolecules. More recently, QELS has been extended to the study of polydisperse systems of small biological scatterers. This extension was made possible by two distinct advances in the analysis of QELS data. In the first, in addition to measuring the average diffusion coefficient, Frederick et al. (3) performed composite empirical fits of Lorentzian curves to QELS power density spectra to ascertain the degree of sample polydispersity. In the second, Pusey et al. (4) using the method of cumulants developed by Koppel (5), measured sample polydispersity as well as the average diffusion coefficient using QELS temporal autocorrelation data. Both approaches have been used extensively since they were introduced.

In this paper, the application of QELS is further extended to include the case of large scatterers (vesicles) in polydisperse suspensions. This is accomplished by explicitly including vesicle size and structure in the expression for the scattered light electric field autocorrelation function and then using the cumulant expansion approach on this expression. The result is a pair of criteria which when satisfied allow polydisperse vesicle suspensions to be considered as polydisperse suspensions of small scatterers. This result is closely related to the conclusion that large scatterers appear to be small scatterers at sufficiently small scattering angles (6, 7).

Using the technique developed in this paper, the researcher can quickly and accurately measure the average diffusion coefficient, and the relative dispersion in the diffusion coefficient about this average, of SR vesicle suspensions. He is thereby provided with a convenient and quantitative means of characterizing vesicle suspension dynamics.

THEORY

In this section, an expression is developed to describe the QELS temporal autocorrelation spectrum of a dilute polydisperse suspension of "model" vesicles. Criteria are then derived to quantitatively define conditions for which (large) vesicles may be treated as small scatterers in QELS experiments.

To accomplish the above, the following assumptions concerning the sample are made:

(*1*) A model vesicle is a rigid spherical shell of radius R_l and vanishingly small thickness comprised of N_e optically isotropic elements each having scalar polarizability, α.

(*2*) Solvent density fluctuations contribute negligibly to scattered field and intensity fluctuations, i.e., the solvent is "invisible."

(*3*) Vesicles in the sample satisfy the criterion (6, 8, 9, 10)

$$2R_l \ll \lambda_o/2\pi(n - n_o), \tag{1}$$

where n and n_o are the vesicle and solvent refractive indices, respectively, and λ_o is the vacuum wavelength of light.

(*4*) The vesicle suspension is effectively infinitely dilute so that the N vesicles in the sample may be treated as moving independently of one another.

(*5*) The vesicle sample/system is both stationary and ergodic.

When these assumptions are satisfied, the scattered electric field autocorrelation function for such a system may be written (11, 12)

$$| g^{(1)}(\tau) | = C^2 \sum_{l=1}^{N} F(KR_l) \exp(-D_l K^2 \tau), \tag{2}$$

where

$$F(KR_l) = \sum_{j,m=1}^{N_e} \exp[i\mathbf{K}\cdot(\mathbf{R}_{jl} - \mathbf{R}_{ml})] \tag{3}$$

is the (time-independent) Debye structure factor for the lth vesicle which describes the interference of all possible pairs of vesicle dipole scattering elements indexed by j and m and as is shown in Appendix I, when the vesicle thickness is vanishingly small

$$F(KR_l) = \sin^2 KR_l / K^2 R_l^2. \tag{4}$$

In addition, $C \equiv \omega_o^2 \alpha E_o / c^2 r$ with ω_o and E_o the circular frequency and electric field amplitude of the incident light, respectively, c the vacuum speed of light, r the distance from sample to observer, and, finally, $\mathbf{K}$ is the scattering vector related to the scattering angle θ (see Fig. 1) in the following way for QELS:

$$K = | \mathbf{K} | = (4\pi n_o / \lambda_o) \sin \theta/2. \tag{5}$$

Thus

$$| g^{(1)}(\tau) | = C^2 \sum_{l} (\sin^2 KR_l / K^2 R_l^2) \exp(-D_l K^2 \tau). \tag{6}$$

To relate R_l and D_l in expression 6, the Stokes-Einstein relation is used,

$$D_l = k_B T / 6\pi\eta R_l, \tag{7}$$

where η and T are the solvent viscosity and absolute temperature, respectively, and k_B is the Boltzmann constant.

For a polydisperse system when D is considered to be a continuous variable, Eq. 7 may be used so that expression 6 can be written in terms of D to read:

$$| g^{(1)}(\tau) | = NC^2 \int_0^\infty G(D)[\sin^2(KA/D)/(KA/D)^2] \exp(-DK^2\tau) \mathrm{d}D, \tag{8}$$

with $G(D)$ the unknown normalized diffusion coefficient distribution function for vesicles such that

$$\int_0^\infty G(D)\mathrm{d}D = 1 \tag{9}$$

and

$$A \equiv k_B T/6\pi\eta. \tag{10}$$

As it stands, Eq. 8 is not very helpful in interpreting light-scattering autocorrelation results. A method which has demonstrated its value in reformulating expressions like 8 so that they become useful is that of the cumulant expansion developed by Koppel (5) and soon thereafter applied to measurements of R17 virus diffusion coefficients by Pusey et al. (4). Using this approach, the integrand—excluding $G(D)$—is expanded in a Taylor series about the modified Z-average diffusion coefficient $<D>$ where

$$<D> = \int_0^\infty G(D)D\mathrm{d}D. \tag{11}$$

Explanations of Z-averaging and modified Z-averaging are given in paragraph *vi* of the Discussion of Results section of the paper.

The result is an expression for $|g^{(1)}(\tau)|$ written in terms of moments of the diffusion coefficient distribution about $<D>$. In general form:

$$|g^{(1)}(\tau)| = NC^2\left\{H(K, <D>, \tau) + \mu_1 \frac{\partial H}{\partial D}\bigg|_{<D>} + \frac{\mu_2}{2!}\frac{\partial^2 H}{\partial D^2}\bigg|_{<D>} + \ldots\right\}, \tag{12}$$

where

$$H = H(K, D, \tau) = [\sin^2(KA/D)/(KA/D)^2]\exp(-DK^2\tau) \tag{13}$$

and $\mu_1 = \int_0^\infty G(D)(D - <D>)\mathrm{d}D \equiv 0$ is the first moment of the distribution, $\mu_2 = \int_0^\infty G(D)(D - <D>)^2\mathrm{d}D$ is the second moment, etc. Specifically,

$$\begin{aligned}|g^{(1)}(\tau)| = {} & NC^2 e^{-\tau/\tau_c}\{(\sin^2 x/x^2) + (\delta_2/2)[(2\sin^2 x/x^2) - (4\sin x\cos x/x) \\ & + 2\cos^2 x - 2\sin^2 x - (4\tau/\tau_c)(\sin^2 x/x^2) \\ & + (4\tau/\tau_c)(\sin x\cos x/x) + (\tau/\tau_c)(2\sin^2 x/x^2)]\},\end{aligned} \tag{14}$$

where the expansion has been carried out through the μ_2 term and the notation has been simplified by using the distribution relative dispersion, $\delta_2 \equiv \mu_2/<D>^2$ and setting $x \equiv KA/<D>$, $\tau_c \equiv 1/<D>K^2$.

By considering only small (1/20 of λ_o/n_o, or smaller) vesicles, i.e., considering x small, then Eq. 14 reduces to:

$$|g^{(1)}(\tau)| = NC^2\exp(-<D>K^2\tau)\left\{1 + \frac{(\mu_2)_\Gamma}{2}\tau^2\right\}. \tag{15}$$

Since $(\mu_2)_\Gamma = K^4\mu_2$, expression 15 agrees with that of Pusey et al. (13) and has been used by them as well as others to study polydisperse suspensions of both small biological scatterers, and small synthetic scatterers (for example, ref. 14).

Oftentimes, and as is the case in this paper, QELS experiments measure intensity autocorrelation rather than field autocorrelation. Then, instead of expression 14, the intensity autocorrelation function, $g^{(2)}(\tau)$, must be formulated.

When the scattered field is a Gaussian random variable, as is the case for the experiments reported here, then $g^{(1)}(\tau)$ and $g^{(2)}(\tau)$ are related through the Siegert equation in a straightforward way (15):

$$g^{(2)}(\tau) = <I>^2 + |g^{(1)}(\tau)|^2, \tag{16}$$

where $<I>^2$ is the square of the average intensity. Since $<I>^2$ is subtracted by our correlator from $g^{(2)}$, the observed autocorrelation spectrum, $\Delta g^{(2)}$ is:

$$\begin{aligned}\Delta g^{(2)}(\tau) &\equiv g^{(2)}(\tau) - <I>^2 \\ &= N^2C^4\frac{\sin^4 x}{x^4}e^{-\tau/\tau_c}\left\{1 + \delta_2\left[\left(\frac{\tau}{2\tau_c} + 2(x\cot x - 1)\right)^2\right.\right. \\ &\quad \left.\left. - 2(x\cot x - 1)^2 - 2x^2\right]\right\},\end{aligned} \tag{17}$$

where now $\tau_c = 1/(2<D>K^2)$ instead of $1/(<D>K^2)$ and terms including δ_2^2 are assumed negligible.

When the small scatterer (small x) limit is considered in expression 17, the expression reduces to that used by Chen et al. (16) in QELS intensity autocorrelation studies of suspensions of meningococcal polysaccharides and by Chu et al. (17) in QELS studies of lactoglobulin suspensions.

As it stands, expression 17 is too complicated to apply to the autocorrelation spectra of light scattered from vesicle suspensions and does not represent much improvement over expression 8. By demanding that

$$\delta_2|\alpha(x,\tau)| \ll 1, \tag{18}$$

however, where

$$\alpha(x,\tau) = [(\tau/2\tau_c) + 2(x\cot x - 1)]^2 - 2(x\cot x - 1)^2 - 2x^2, \tag{19}$$

then $1 + \delta_2\alpha(x,\tau) \simeq \exp[\delta_2\alpha(x,\tau)]$ and Eq. 17 simplifies to

$$\Delta g^{(2)}(\tau) \simeq B^2 e^{-\tau/\tau_c} e^{\delta_2\alpha(x,\tau)}, \tag{20}$$

where

$$B \equiv NC^2(\sin^2 x/x^2). \tag{21}$$

By considering $ln\Delta g^{(2)}$, as is usually done, then

$$ln\Delta g^{(2)}(\tau) = d + b\tau + a\tau^2, \tag{22}$$

where

$$d = 2\ln B + 2\delta_2[(x\cot x - 1)^2 - x^2], \tag{23}$$

$$b = (1/\tau_c)[2\delta_2(x\cot x - 1) - 1], \tag{24}$$

and

$$a = \delta_2/4\tau_c^2 = \mu_2 K^4. \tag{25}$$

Because semi-log plots of our vesicle autocorrelation spectra are distinctly quadratic in character—any higher degree behavior being "lost" in spectral noise—Eq. 22 has been used to interpret these spectra (see Fig. 2 for a photograph of a typical autocorrelation function). By fitting a second degree polynomial to (base-line corrected) $\ln\Delta g^{(2)}$ vs. τ data, the fit parameters a, b, and d are determined and then from a and b, $<D>$ and μ_2 are calculated using Eqs. 24 and 25.

As shown in Appendix II, when the restriction $\delta_2 \mid \alpha(x, \tau) \mid \ll 1$ is satisfied, and if

$$x^2 \ll 1/2\delta_2, \tag{26}$$

with

$$\delta_2 \leq 0.5, \tag{27}$$

then necessarily

$$\mid x\cot x - 1 \mid \ll 1/\delta_2. \tag{28}$$

Applying 28 to Eq. 24,

$$b \simeq -1/\tau_c \tag{29}$$

so that

$$<D> \simeq -b/2K^2 \tag{30}$$

and

$$\mu_2 = a/K^4 \quad \text{as before.} \tag{31}$$

The simplified results 30 and 31 correspond, as far as the coefficients a and b are concerned, to measurements of suspensions of small, polydisperse Rayleigh scatterers. This is because the "structure factor" term in b, namely $x\cot x - 1$, has been made negligible in Eq. 24 by forcing $\delta_2 \mid \alpha(x, \tau) \mid \ll 1$.

The significance, then, of this theoretical development has been to provide a pair of quantitative criteria, specifically relations 18 and 28 which when satisfied for a given τ allow polydisperse suspensions of large spherical-shell scatterers to be treated as polydisperse suspensions of small scatterers in QELS correlation spectroscopy.

EXPERIMENT

Sample Preparation

Sarcoplasmic reticulum vesicles were isolated from lobster abdominal muscles by a method that has been previously described in ref. 1. QELS analysis and EM sample

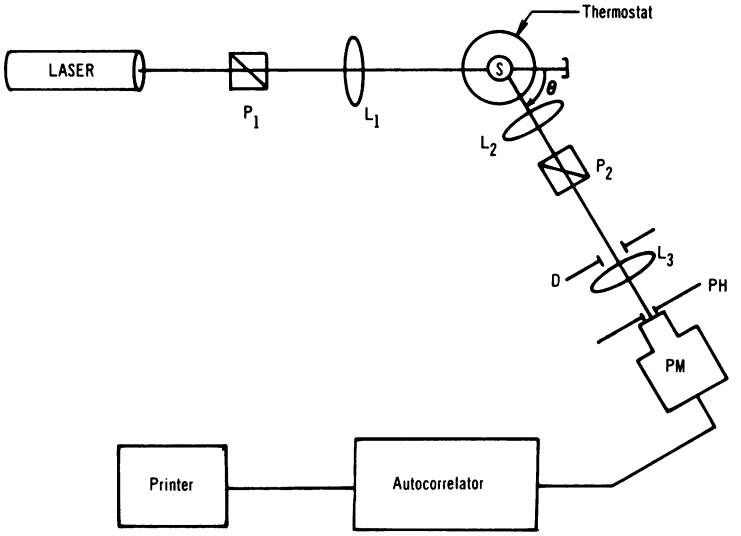

FIGURE 1 Top view illustration of the QELS experimental arrangement where L denotes lens; P, polarizer; D, diaphragm; S, sample; PH, pinhole; and PM, photomultiplier. Both polarizers are set to pass vertically (perpendicular to the plane of the paper) polarized light.

preparation were accomplished within hours of vesicle isolation. The activity of sample vesicles was monitored. Calcium uptake was determined by introducing an aliquot of calcium into the reaction mixture and then determining the time course of ATPase activity.[1] In turn, ATPase activity was measured using a pH method described in Nishimura et al. (18).

Prior to analysis by QELS and EM, vesicles were sonicated to achieve as homogeneous a distribution as possible and to minimize vesicle aggregation. Dilute suspensions were sonicated in an ice bath for 10 periods of 20 s each. Each period was followed by a 1–2 min interval. In addition, calcium transport was monitored after sonication and no decrease in calcium transport activity was observed.

Sonication of vesicle suspensions prior to their study using QELS is essential. Earlier experiments without sonication invariably gave unreasonably large estimates of inferred (see Discussion of Results) vesicle size. This was most likely due to the association of vesicles into dimers, trimers, and perhaps even larger aggregates.

To reduce the dust contribution to noise in subsequent QELS analysis, the suspension buffer (10 mM TES) was filtered five times each through two 0.2 μm Millipore filters just before the vesicle suspension was brought to final dilution.

The scattering (final dilution) sample had a protein concentration of 0.40 mg/ml. At this concentration, the nearest (on the average) that two scattering elements of different vesicles approach each other is 2,131 Å while the hard-sphere collision fre-

[1] Baskin, R. J. In preparation.

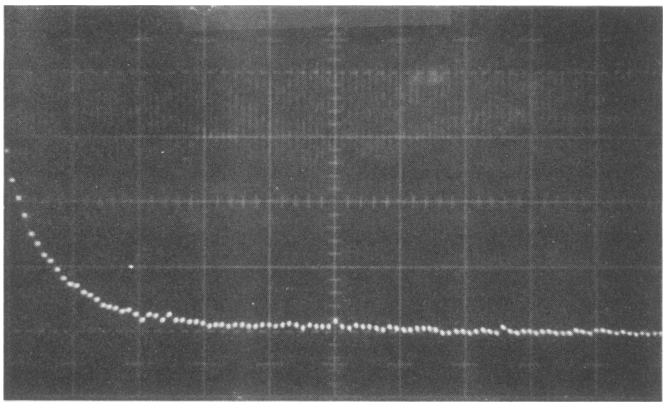

FIGURE 2 Photograph of a typical correlation function spectrum. Here the data corresponds to a $\theta = 16°$ run. The ordinate axis is in arbitrary units. The abcissa corresponds to 20 ms/1 cm. division.

quency of these vesicles is sufficiently small (68/s per vesicle) that vesicles may be considered to be diffusing freely in suspension (see Appendix IV).

Scattering Apparatus

A schematic of the scattered light measurement apparatus is presented in Fig. 1. The set up is, for the most part, the conventional one with the following exceptions: (*a*) Because of the postsample optics, an accurate visual estimate of the scattering volume can be made. (*b*) The scattering cell (Precision Cells, Inc., Hicksville, N.Y.) is especially constructed to ensure uniformity of its cylindrical shape and its wall thickness and is manufactured of Suprasil quality fused quartz to eliminate spurious cell-wall fluorescence in the scattered signal. (*c*) The correlator (Saicor model SAI-42; Honeywell, Hauppauge, N.Y.) was used solely in the unclipped mode.

Measurements

Eight measurements of $\Delta g^{(2)}$ were made at scattering angles of 20, 18, 16, 14, 12, and 10 degrees—in that order—over a period of 6 hr. Dual measurements at different correlator lag times were made "back to back" at 12° to check the effect of this difference on the measurement of $\Delta g^{(2)}$. Two 20° measurements were also made—the very first measurement in the set at 4 p.m. and the very last measurement at 10 p.m.—to check the stability of the sample. For all eight experimental runs, the sample was thermostatically maintained at 12.5°C and the laser power was kept at a constant 10 mW. A stabilized argon-ion laser emitting at 5,145 Å and operating in the TEM_{oo} mode was used as the incident light source.

Spectral base-line estimates were made by averaging over at least the last 10 correlation function values (bins) when the function had clearly settled down and flattened.

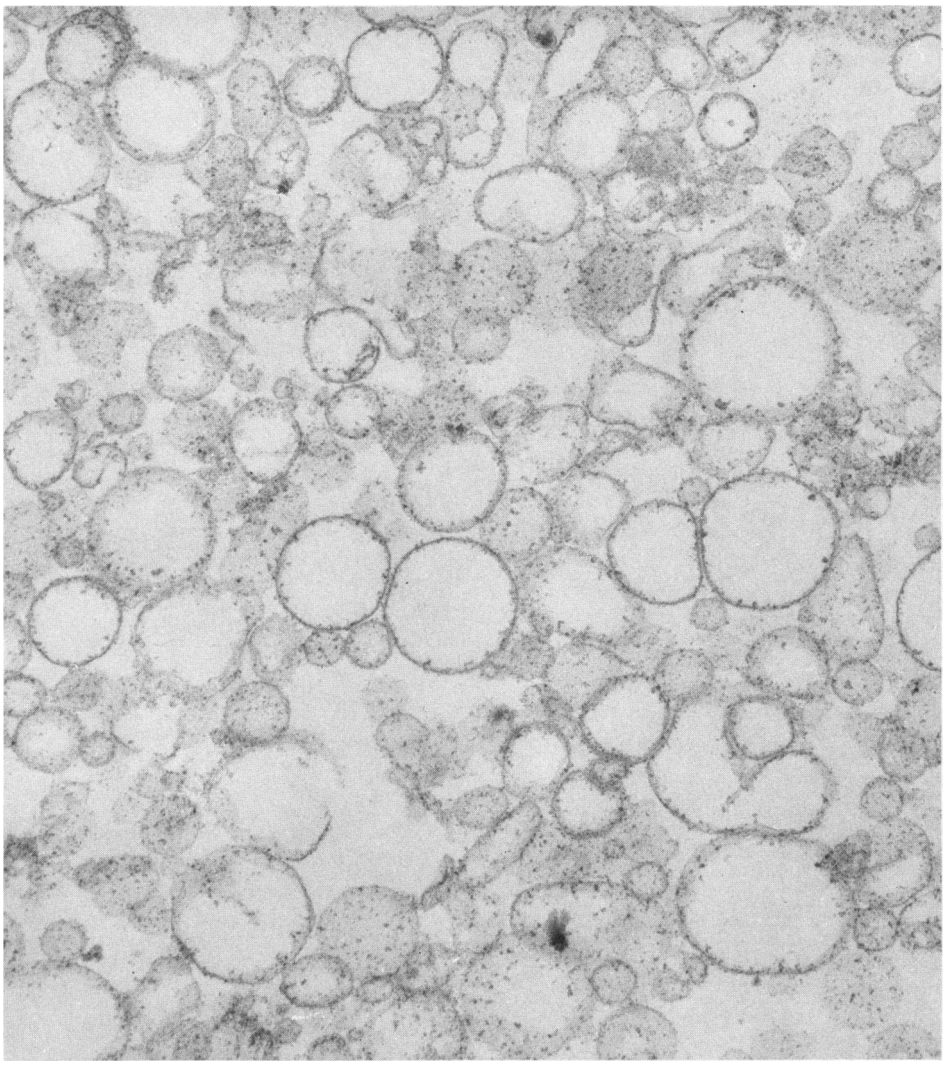

FIGURE 3 Thin-section electron micrograph of the vesicle preparation used in the QELS and EM measurements reported in this paper.

In Fig. 2, for example, the base line was determined by averaging bins 80–99. If, however, for any run the correlation function had not clearly flattened, the run was reaccomplished at the next higher lag-time setting so that, in effect, the correlation spectrum was squeezed up against the ordinate resulting in a longer base-line "tail"—*then* at least the last 10 bins were averaged. This approach provided well-defined base-line estimates for all runs (see QELS Results in the following section for discussion concerning the effect of base-line uncertainty on spectral fits).

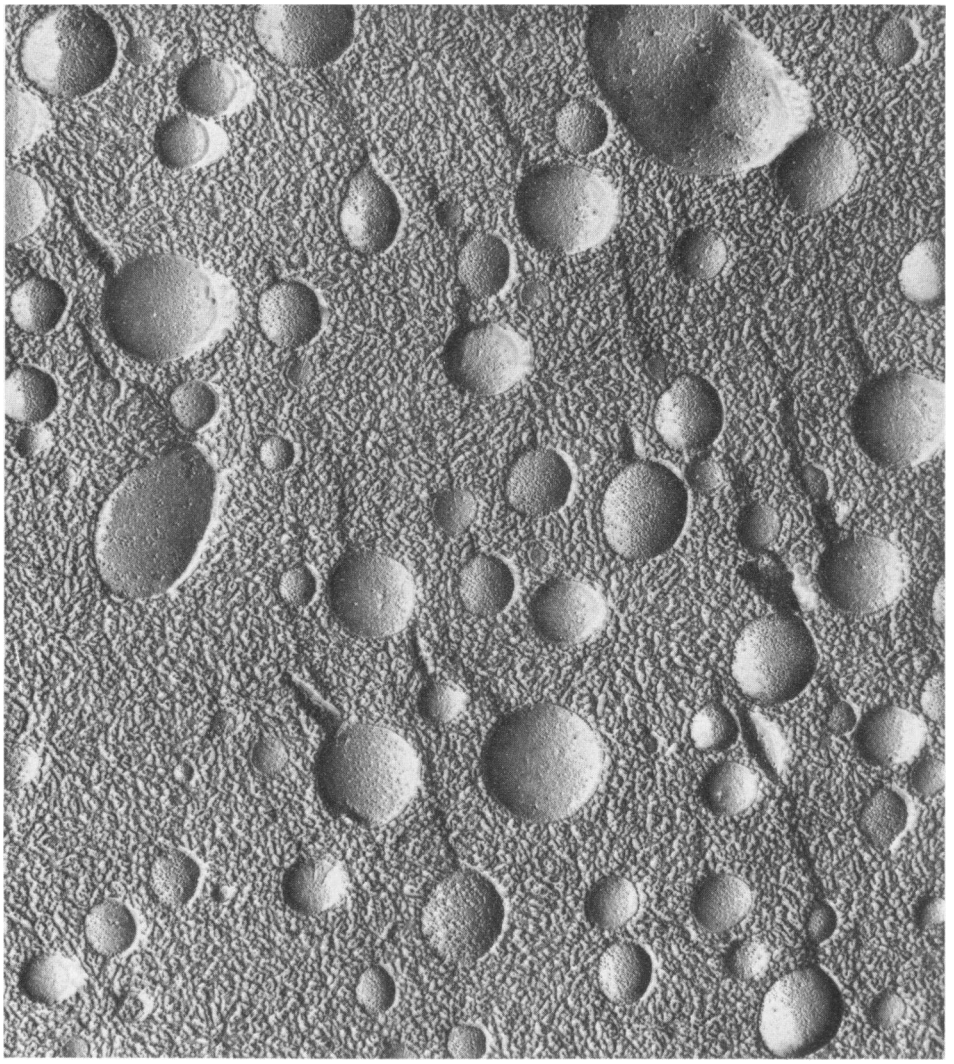

FIGURE 4. Freeze-etch electron micrograph of the vesicle preparation used in the QELS and EM measurements reported in this paper.

DISCUSSION OF RESULTS

EM Results

The final dilution, sonicated vesicle suspension was split and half was analyzed using QELS while the other half was analyzed using EM. EM samples were prepared both by thin-sectioning (1) and by freeze-etch (2). In both cases, the sizes of 400–500 vesicles were measured using micrographs made at a final magnification of 69,445 (see Figs. 3 and 4). The final size estimations were taken from the thin-section micrographs.

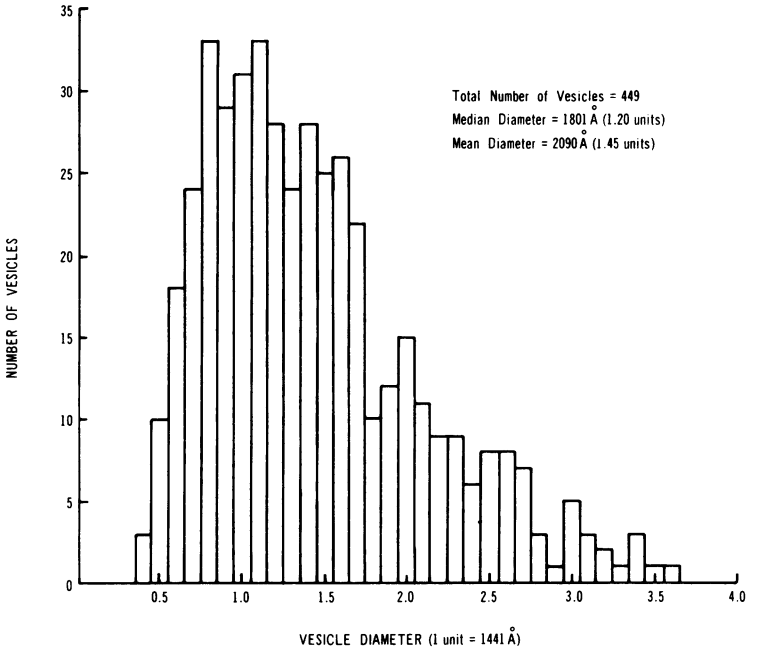

FIGURE 5 Frequency histogram of vesicle sizes made using individual measurements of 449 vesicles from a thin-section electron micrograph having magnification 69,445.

The average vesicle radius was found to be $<R>$ = 1,045 Å with a root-mean-square deviation about this average of σ_R = 491 Å. A frequency-size histogram of these EM measurements is presented as Fig. 5, and a comparison of these results with those of QELS is given in paragraph *vi* below.

Arrio et al. (19) first used both QELS and EM to analyze (rabbit) SR vesicle suspensions—although they did not account for vesicle size or polydispersity in their calculations. Furthermore, their estimates of vesicle size were based to a considerable extent on measurements of negatively stained vesicles. The negative stain technique is known to cause vesicle shrinkage and gross shape distortion (2). Pictures in Arrio et al. show many vesicles with altered shape (e.g., Fig. 2 of ref. 19).

QELS Results

The eight sets of QELS autocorrelation data were fitted both linearly (subscripted by 1) and quadratically (subscripted by 2) for a maximum number of correlator lag times $\tau_{max} = \tau_c$ (Table I) and then refitted for $\tau_{max} = 3/2\tau_c$ (Table II). The uncertainties reported in Tables I and II reflect the variances of and the covariance between the fit parameters a and b as determined by curve fitting the data (see Appendix II). Since the data are presumed to be of the form $\ln \Delta g^{(2)} = d + b\tau + a\tau^2$, the reported uncertainties are assumed to reflect all sources of error in the measurement of $\Delta g^{(2)}$ where $\Delta g^{(2)}$ values were base-line corrected to eliminate unwanted contributions to the

TABLE I

QELS RESULTS FOR BOTH LINEAR AND QUADRATIC DATA FITS WITH THE MAXIMUM ALLOWED CORRELATOR LAG TIME EQUAL TO ONE COHERENCE TIME, $\tau_c(\tau_{max} = \tau_c)$

θ	$\langle D \rangle_1 \times 10^8$	σ_1	$\langle D \rangle_2 \times 10^8$	σ_2	$\mu_2 \times 10^{17}$	δ_2	Lag Time	No. of Fit Points
°	cm^2/s		cm^2/s		cm^4/s^2		ms	
10	1.38±0.05	3.79×10^{-2}	1.97±0.10	1.63×10^{-2}	26.5±4.4	0.684±0.049	5	10
12	1.50±0.03	2.31×10^{-2}	1.83±0.11	1.41×10^{-2}	14.3±4.7	0.427±0.090	5	7
12	1.43±0.02	1.50×10^{-2}	1.66±0.04	8.68×10^{-3}	11.7±2.2	0.423±0.060	2	16
14	1.44±0.02	1.71×10^{-2}	1.66±0.07	1.21×10^{-2}	11.1±3.4	0.402±0.089	2	12
16	1.60±0.04	2.50×10^{-2}	1.90±0.15	2.04×10^{-2}	14.9±7.0	0.409±0.132	2	9
*18	1.60±0.02	1.70×10^{-2}	—	1.78×10^{-2}	—	—	1	13
*20(4P.M.)	1.66±0.02	1.25×10^{-2}	1.76±0.08	1.20×10^{-2}	5.45±4.04	0.176±0.115	1	11
*20(10P.M.)	1.71±0.03	2.00×10^{-2}	—	1.67×10^{-2}	—	—	1	10

spectrum of (principally) dust and larger vesicle aggregates. Because of the high quality of our correlation spectra, we assumed throughout that uncertainties in our base-line estimates could safely be ignored, i.e., we presumed that we knew exactly what our base lines were. We checked this assumption by twice analyzing the 10° run data for $\tau_{max} = \tau_c$ using base lines of five and zero, respectively. The differences between the resulting $\langle D \rangle$ and δ_2 values and their respective uncertainties were insignificant. This insensitivity to base-line fluctuation for $\tau_{max} = \tau_c$ results is discussed further in paragraph *ii-a* below.

For purposes of analysis, $|\alpha(x, \tau)| \ll 1/\delta_2$ was taken to mean

TABLE II

QELS RESULTS FOR BOTH LINEAR AND QUADRATIC DATA FITS WITH THE MAXIMUM ALLOWED CORRELATOR LAG TIME (τ_{max}) EQUAL TO $3/2\,\tau_c$

θ	$\langle D \rangle_1 \times 10^8$	σ_1	$\langle D \rangle_2 \times 10^8$	σ_2	$\mu_2 \times 10^{17}$	δ_2	Lag Time	No. of Fit Points
°	cm^2/s		cm^2/s		cm^4/s^2		ms	
*10	1.23±0.04	4.81×10^{-2}	—	2.20×10^{-2}	—	—	5	15
*12	1.32±0.04	4.98×10^{-2}	1.80±0.08	2.18×10^{-2}	14.0±2.2	0.430±0.033	5	11
12	1.38±0.02	2.68×10^{-2}	1.48±0.07	2.60×10^{-2}	3.56±2.35	0.163±0.092	2	24
14	1.40±0.01	2.05×10^{-2}	1.56±0.05	1.58×10^{-2}	5.46±1.57	0.224±0.051	2	18
16	1.50±0.03	3.70×10^{-2}	1.87±0.09	2.38×10^{-2}	13.0±3.2	0.372±0.055	2	13
18	1.55±0.01	1.91×10^{-2}	1.63±0.06	1.87×10^{-2}	2.83±2.12	0.106±0.072	1	20
20(4P.M.)	1.62±0.06	1.86×10^{-2}	1.79±0.06	1.46×10^{-2}	6.79±2.25	0.212±0.057	1	15
20(10P.M.)	1.62±0.02	2.80×10^{-2}	1.91±0.07	1.80×10^{-2}	10.8±2.4	0.296±0.045	1	16

$$10 \mid \alpha(x, \tau) \mid \leq 1/\delta_2. \tag{32}$$

Asterisks in the tables indicate which quadratic fits did not satisfy condition 32, although results for those runs almost satisfying this restriction were calculated and presented for comparison purposes anyway.

(*i*) The most obvious results common to Tables I and II are:

(*a*) $<D>_1$ increases monotonically with increasing θ (the first 12° run in Table I excepted), whereas $<D>_2$ values do not. Since the effect of vesicle size on the spectra was eliminated using the criteria discussed earlier, the dependence of $<D>_1$ on angle results solely from vesicle polydispersity. In short, $<D>_2$ results take polydispersity into account whereas $<D>_1$ results do not; for this reason and reasons given below, $<D>_2$ values are taken to be the valid estimates of the true average vesicle diffusion coefficient.

(*b*) Based on the goodness of fit parameter σ (Tables I and II) where σ is the "standard deviation of the fit,"

$$\sigma = \sum_{i=1}^{N} (y_i - P(x_i))^2/(N - m - 1) \tag{33}$$

with y_i the set of N values of $\ln \Delta g^{(2)}$, $P(x_i)$ the corresponding calculated regression polynomial values and m the degree of the fit polynomial—the data are better fitted to second degree polynomials than first with the exception of the 18° run in Table I.

(*c*) The uncertainties associated with $<D>_1$ values are less than those associated with corresponding $<D>_2$ values giving the impression that $<D>_1$ values are more accurate than corresponding $<D>_2$ values. In fact, the two types of uncertainties cannot be directly compared. This can be seen by comparing the roles of b (since $<D> \simeq -b/2K^2$ in both cases) in the linear and quadratic fit equations. For a linear fit

$$\ln \Delta g^{(2)} = d + b\tau, \tag{34}$$

thus, b is the relatively well defined slope of a straight-line fit to data that actually describe a very "shallow" parabola and thus uncertainty in b results from uncertainty in estimating this slope. By contrast, for a quadratic fit,

$$\ln \Delta g^{(2)} - [d - (b^2/4a)] = a[\tau + (b/2a)]^2 \tag{35}$$

(in normal form) and b (with a) determines both the vertex and the focus of this fit parabola so that uncertainties in b in this case reflect uncertainties in both of these parabolic parameters. In addition, it is seen that a and b are correlated.

(*d*). Although the relative dispersion, δ_2, depends on the second moment and the diffusion coefficient as

$$\delta_2 = \mu_2/<D>_2^2, \tag{36}$$

uncertainties in δ_2 are actually smaller than corresponding uncertainties in μ_2. This

results from the negative linear correlation between a and b and is explained in detail in Appendix II.

(*e*) The greatest uncertainties in the results are those for μ_2. From expression 35, it is seen that a, in addition to determining with b the parabolic focus and vertex, also determines (alone) the curvature of the fit parabola. Since $\mu_2 = a/K^4$, uncertainties in μ_2 reflect all three sources of uncertainty in a.

(*ii*) Concentrating on quadratic results, the most obvious differences between Table I and II are:

(*a*) Though fewer data points are used for Table I results, Table I fits (σ_s) are better than those of Table II. This is because data beyond $\tau_{max} \simeq \tau_c$ are proportionately more noisy than data with $\tau \lesssim \tau_c$. Since a, as a measure of parabolic curvature, is particularly sensitive to noise (dust, vesicle aggregates, etc.) and this sensitivity is transmitted to b because a and b are strongly negatively correlated, inclusion of data points beyond $\tau \simeq \tau_c$ adversely affects estimates of both a and b and thus of μ_2, δ_2 and $<D>_2$. On the other hand, the maximum number of data points that can be accommodated up to $\tau \simeq \tau_c$ should be taken. In our situation, this maximum number was determined by the available lag-time settings of the correlator (i.e., 1, 2, and 5 ms for the sample in question) and by necessity of determining a well-defined base line in 100 correlator lag times. With additional correlator settings of, say, 3, 4, 6, 7, and 8 ms, we probably could have obtained at least 15 points/run—all having $\tau_{max} \lesssim \tau_c$. An example of such an "optimum" run turned out to be the second 12° run (incorporating 16 points) in Table I. For this reason, a plot of $\ln \Delta g^{(2)}$ vs. τ for this run showing both linear and quadratic fits for comparison is presented as Fig. 6.

(*b*) Values in Table II exhibit more variability than those in Table I. In addition, Table II $<D>_2$ and δ_2 values are smaller when a large number of data points were used in their estimation, and vice-versa, whereas in Table I this is not the case. We feel that both the increased variability and the data-point number dependence of Table II result from noise effects on a (and thus on b) due to the enhanced nature of noise contributions to the auto-correlation spectrum beyond $\tau \simeq \tau_c$. A specific example of strange behavior in Table II that is not found in Table I is that of the set of two 12° runs. In Table II, a larger number of data points used to fit the data resulted in a *worse* fit (smaller σ) and in *greater* uncertainty in δ_2. For the same set in Table I, a greater number of points yielded the expected results of better fit and smaller uncertainties in both δ_2 and $<D>_2$.

(*iii*) The correlator check at 12°—using Table I results—demonstrated that the correlator measures the same sample at (about) the same time in essentially the same way, whether the correlator lag time is 2 ms or 5 ms.

(*iv*) A check on the stability of the sample by comparing 20° 4 p.m. and 10 p.m. results failed because although results for the $\tau_{max} = 3/2\tau_c$ case satisfied the criteria 18 and 28, for both runs, these values were not considered reliable for reasons given earlier. In addition, when $\tau_{max} = \tau_c$, neither run could satisfy the criteria 18 and 28 so a comparison could not be made.

(*v*) Our best estimates of $<D>_2$ and δ_2 were made using Table I results and invoking the acceptance criteria 18 and 28. The 10° point in Table I was not included in the determination of the averaged $<D>_2$ because of its calculated excessively large δ_2. We believe that a possible reason for this large δ_2 is that the combination of longer time lag scans and the larger scattering volume, both necessary at smaller scattering angles, favors anomalously high dispersion estimates because of large aggregates and/or dust particles in the sample. So, weighted average values of $<D>_2$ and δ_2 were calculated using both 12° results and the 14° and 16° results. Individual values were weighted with their respective normalized reciprocal variances and the reciprocal of the overall variance was computed as the sum of the reciprocals of the individual variances. The results are

$$\overline{<D>}_2 = (1.69 \pm 0.03) \times 10^{-8}\ \text{cm}^2/\text{s} \tag{37}$$

and

$$\bar{\delta}_2 = 0.418 \pm 0.041. \tag{38}$$

Our choice of δ_2 rather than μ_2 as the principle parameter to measure polydispersity follows from two considerations: (*a*) δ_2 is a more tractable parameter than μ_2 because it is dimensionless and of order 1; (*b*) δ_2 can be estimated more accurately than μ_2 due to the strong negative linear correlation between a and b (see Appendix II).

(*vi*) In light-scattering experiments on polydisperse suspensions of small, i.e., $2R < \lambda_o/20n_o$, scatterers, it is the so-called Z-average diffusion coefficient that is measured (7, 15, 20). Then

$$<D> = \sum_i N_i M_i^2 D_i \Big/ \sum_i N_i M_i^2, \tag{39}$$

where N_i and M_i specify the number and masses, respectively, of scatterers in the scattering volume having diffusion coefficient D_i.

For larger scatterers, e.g., vesicles which do not satisfy the condition $2R < \lambda_o/20n_o$ but do satisfy the condition 1, the Z-averaging must be modified to include the scatterer structure factor (14). Then

$$<D> = \sum_i N_i M_i^2 F(x_i) D_i \Big/ \sum_i N_i M_i^2 F(x_i) \tag{40}$$

with $F(x_i)$ the structure factor where $x_i = KR_i$.

Thus it is a remarkable coincidence that our modified, Z-averaged diffusion coefficient yields an inferred vesicle size,

$$R_2 \equiv k_B T/6\pi\eta <D>_2, \tag{41}$$

which is very close to the number averaged EM size estimate, $<R>$. Specifically,

$$<R> = 1{,}045\ \text{Å} (\delta_R = 0.221), \tag{42}$$

$$R_2 = 1{,}041\ \text{Å}. \tag{43}$$

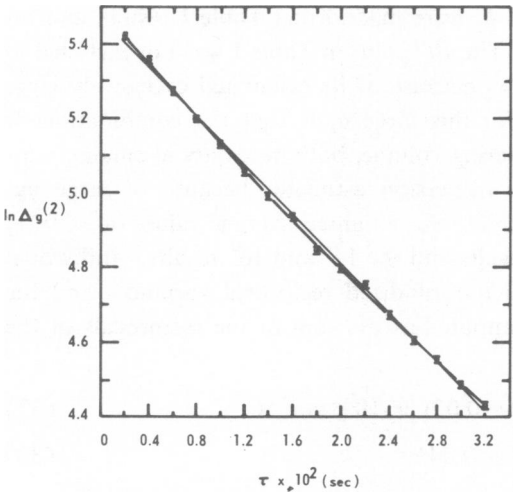

FIGURE 6

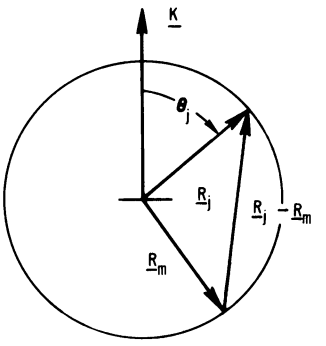

FIGURE 7

FIGURE 6 Linear (thin line) and quadratic (thick line) fits to the 16 point Table I 12° scattering angle data. The error bars represent the magnitude of the goodness of fit parameter, σ, for the quadratic fit.

FIGURE 7 Schematic illustrating the geometry used to carry out the integration in expression 46. The indices j and m identify two arbitrary scattering elements whose (constant magnitude) position vectors are related through their orientation with respect to the reference scattering vector, **K**.

(*vii*) The derivation of the structure factor given in Appendix I depends on the fact that the condition $2R \ll \lambda_o/2\pi(n - n_o)$ is met. Again, as stated at the beginning of the theory section, we have assumed that the refractive indices of sample buffer and vesicles are sufficiently close that condition 1 is met.

CONCLUSIONS

The technique developed in this paper (applying the criteria given by Eqs. 18 and 28 and restricting τ such that $\tau_{max} \leq \tau_c$) enables QELS to be used to measure the modified Z-bar average diffusion coefficient and the relative dispersion in the diffusion coefficient about this average for dilute, polydisperse SR vesicle suspensions. In effect, this approach allows vesicle suspensions to be treated in QELS as suspensions of point-scatterers and in this way extends the size range of application of QELS for such systems from the upper limit imposed by the Rayleigh criterion, $2R \leq \lambda_o/20n_o$, to that imposed by the criterion 1.

The technique can be used for QELS analysis of any vesicle suspension whose solvent is "invisible" provided:

(*a*) The suspension is sufficiently dilute so that, practically speaking, scatterers scatter light independently and diffuse freely in a coherence time.

(*b*) The suspension does not significantly depolarize light in the scattering process.

(*c*) It is known, presumably from EM analysis of experiments on "standardized" suspensions, that the criterion 1 is met. In this respect, being able both to match solvent and vesicle refractive indices and to choose a laser with a long wavelength emission line extends experimental capability significantly.

(*d*). Sample vesicles are known to be spherical shells whose thickness is small compared with the wavelength of the incident laser light in the sample solvent.

Our results show that by making several measurements and using the experimental and analytical methods presented in this paper, $<D>_2$ can be measured with an accuracy of about 2% and δ_2 can be measured with an accuracy of about 10%. This ability to accurately measure $<D>_2$ and δ_2 demonstrates that QELS can be used to follow vesicle size and conformation changes—at least for certain processes. For example, once $<D>_2$ and δ_2 are determined for a particular vesicle suspension, then any changes in vesicle size due to osmotic pressure changes across vesicle membranes would result in measurable changes in $<D>_2$ and δ_2.

Finally, the technique developed here to extend QELS vesicle suspension analysis capability from the small scatterer (Rayleigh) limit to the limit imposed by condition 1 can itself be extended to spherical shells of arbitrary thickness (to include solid spheres) by substituting the more general structure factor for such shells (derived in refs. 12 and 21) into Eq. 2. This more general approach would yield criteria analagous to Eqs. 18 and 28 which could then be used to identify those experimental situations where (arbitrarily thick) large spherical shells could be considered as small scatterers. In this way, the average diffusion coefficient and the relative dispersion in diffusion coefficient about this average could be determined.

APPENDIX I

From expression 3, the structure factor for the *l*th vesicle is

$$F(KR_l) = \sum_{j,m} \exp[i\mathbf{K}\cdot(\mathbf{R}_{jl} - \mathbf{R}_{ml})]. \tag{3}$$

Since in the Debye treatment, scattering elements are considered to be independent (a valid assumption as long as condition 1 is satisfied), then

$$F(KR_l) = \sum_{j} \exp(i\mathbf{K}\cdot\mathbf{R}_{jl}) \sum_{m} \exp(-i\mathbf{K}\cdot\mathbf{R}_{ml}). \tag{44}$$

Because the "model" vesicle is assumed to be an infinitely thin spherical shell composed of a uniform, continuous distribution of identical infinitesimal scattering elements, Eq. 44 becomes:

$$F_l(KR) = \int \exp(i\mathbf{K}\cdot\mathbf{R}_1) f_1(\mathbf{R}_1)\mathrm{d}\mathbf{R}_1 \int \exp(-i\mathbf{K}\cdot\mathbf{R}_2)\, F_2(\mathbf{R}_2)\mathrm{d}\mathbf{R}_2 \tag{45}$$

$$= \left| \int \exp(i\mathbf{K}\cdot\mathbf{R}) f(\mathbf{R})\mathrm{d}\mathbf{R} \right|^2 \tag{46}$$

where for the "model" vesicle $f(\mathbf{R}) = \delta(|\mathbf{R}| - R_l)/4\pi R^2$, $\delta(\ )$ the Dirac delta function, and correspondingly, $\mathrm{d}\mathbf{R} = R^2 \sin\theta \mathrm{d}\theta \mathrm{d}\phi \mathrm{d}R$, the individual infinitesimal element volume in spherical polar coordinates.

Taking advantage of vesicle spherical symmetry, the integration in Eq. 46 is conveniently carried out using the geometry illustrated in Fig. 7. So

$$\int e^{i\mathbf{K}\cdot\mathbf{R}} f(\mathbf{R})\,d\mathbf{R} = \int_0^{2\pi} d\phi \int [\delta(|\mathbf{R}| - R_l)/4\pi R]\,dR \int_0^{\pi} e^{iKR\cos\theta} R\sin\theta\,d\theta, \quad (47)$$

$$= \tfrac{1}{2}\int [\delta(|\mathbf{R}| - R_l)/R]\,dR \int_{-R}^{R} e^{iKq}\,dq, \quad (48)$$

$$= \int (\sin KR/KR)\,\delta(|\mathbf{R}| - R_l)\,dR, \quad (49)$$

$$= \sin KR_l/KR_l, \quad (50)$$

where in step 48, $q \equiv R\cos\theta$.

Finally,

$$F(KR_l) = \sin^2 KR_l/K^2R_l^2. \quad (4)$$

This result agrees with that derived in a somewhat different fashion by Pecora and Aragón (12) and Tinker (21) for spherical shells whose thickness is made vanishingly small.

APPENDIX II

If condition 18 is satisfied, then

$$|\alpha(x,\tau| = |[(\tau/2\tau_c) + 2(x\cot x - 1)]^2 - 2(x\cot x - 1)^2 - 2x^2| \ll 1/\delta_2. \quad (19)$$

For $\tau = 0$,

$$|\alpha(x,0)| = |2(x\cot x - 1)^2 - 2x^2| < |\alpha(x,\tau)| \ll 1/\delta_2,$$

so

$$(x\cot x - 1)^2 \ll (1/2\delta_2) + x^2. \quad (51)$$

When $x^2 \ll 1/2\delta_2$ then

$$|x\cot x - 1| \ll (1/2\delta_2)^{1/2} \le 1/2\delta_2 \quad \text{for} \quad \delta_2 \le 0.5,$$

so that the condition

$$|x\cot x - 1| \ll 1/2\delta_2 \quad (28)$$

necessarily holds when

$$x^2 \ll 1/2\delta_2 \quad (26)$$

and

$$\delta_2 \le 0.5. \quad (27)$$

Note, however, that condition 28 *may* hold even if conditions 26 and 27 are not met.

APPENDIX III

The uncertainties in $<D>$, μ_2 and δ_2 reported in Table I of the results section are fit "errors" derived from the variance-covariance matrix calculated by a CDC 6600 computer in performing first and second degree polynomial regression fits to the base-line corrected $\ln \Delta g^{(2)}$ vs. τ data sets.

Specifically, since $<D> = -b/2K^2$ in all cases considered, the reported fractional uncertainty in $<D>$ is just that of b, i.e., σ_b/b where the variance of b, σ_b^2, is the (2, 2) element of the variance-covariance (VC) matrix. Likewise, for second degree fits, $\mu_2 = a/K^4$ and the fractional uncertainty in μ_2 is σ_a/a where σ_a^2 is the VC matrix (3, 3) element. Finally, the uncertainty in δ_2 is computed by first writing the relationship between a, b, and δ_2, viz:

$$\delta_2 = \mu_2/<D>^2 = 4a/b^2 \tag{52}$$

and then finding the variance in δ_2, $\sigma_{\delta_2}^2$, using the expression (second and higher order errors negligible) (22):

$$\sigma_Z^2 = (\partial Z/\partial x)^2 \sigma_x^2 + (\partial Z/\partial y)^2 \sigma_y^2 + 2\sigma_{xy}^2 (\partial Z/\partial x)(\partial Z/\partial y), \tag{53}$$

with $Z = Z(x, y)$ and σ_{xy}^2 the covariance between x and y. The result is

$$\sigma_{\delta_2}^2 = (4/b^2)^2 [\sigma_a^2 + (2a/b)^2 \sigma_b^2 - 2\sigma_{ab}^2 (2a/b)], \tag{54}$$

where for second degree fits, σ_{ab}^2 is the covariance between the fit parameters a and b and is both the (3, 2) and (2,3) elements of the (symmetric) VC matrix.

APPENDIX IV

For an average vesicle number density, ρ_n, the average center-to-center vesicle spacing is $s = (1/\rho_n)^{1/3}$. The closest (on the average) two dipole elements on different vesicles approach each other is $s - 2 <R>$ where $<R>$ is the average vesicle radius. Using a vesicle protein weight of 3×10^{-17} g (estimated typical SR vesicle protein weight in ref. 23), a protein concentration of 0.40 mg/ml corresponds to $\rho_n = 1.33 \times 10^3/\text{cm}^3$. Using the EM result $<R> = 1{,}045$ Å, then $s - 2 <R> = 2{,}131$ Å.

Using another approach to get some additional feel for the effect of concentration on vesicle diffusion, we consider Λ—the vesicle (hard sphere) mean free path in suspension—and equate it to the root-mean-square distance, d_{rms}, a vesicle diffuses in a time, t. Then (24)

$$\Lambda = 1/(\sqrt{2}\rho_n \sigma_{\text{HS}}) = d_{\text{rms}} = (6Dt)^{1/2} \tag{55}$$

where $\sigma_{\text{HS}} \equiv$ the vesicle hard sphere cross section $= \pi(2R)^2$ so that

$$t = (192\, D\pi^2 \rho_n^2 R^4)^{-1}. \tag{56}$$

Then using the QELS result $<D>_2 = 1.69 \times 10^{-8}$ cm^2/s and the EM result $<R> = 1{,}045$ Å, we find

$$t = 1.47 \times 10^{-2}\,\text{s} \sim \tau_c = 3.69 \times 10^{-2}\,\text{s}, \tag{57}$$

with τ_c calculated for $\theta = 10°$ where its value is a maximum. The corresponding frequency of vesicle collisions is then

$$\nu = 1/t \simeq 68/\text{vesicle/s}. \quad (58)$$

This work was supported in part by grant BMS73-06918 from the National Science Foundation (J. C. Selser and Y. Yeh) and in part by grant HL12978-06 from the National Heart and Lung Institute (R. J. Baskin).

Received for publication 6 May 1975 and in revised form 25 July 1975.

REFERENCES

1. BASKIN, R. J. 1971. Ultrastructure and calcium transport in crustacean muscle microsomes. *J. Cell Biol.* **48**:49.
2. DEAMER, D. W., and R. J. BASKIN. 1969. Ultrastructure of sarcoplasmic reticulum preparations. *J. Cell Biol.* **42**:296.
3. FREDERICK, J. E., T. F. REED, and O. KRAMER. 1971. The effect of polydispersity on Rayleigh line-broadening measurements of diffusion constants of random coil macromolecules. *Macromolecules.* **4-2**:242.
4. PUSEY, P. N., D. W. SCHAEFER, D. E. KOPPEL, and R. D. CAMERINI-OTERO. 1972. A study of the diffusion properties of R17 virus by time-dependent light scattering. *J. Phys.*(Paris) **33**:C1-163.
5. KOPPEL, D. E. 1972. Analysis of macromolecular polydispersity in intensity correlation spectroscopy: the method of cumulants. *J. Chem. Phys.* **57**:4814.
6. DEBYE, P. 1944. Light scattering in solutions. *J. Appl. Phys.* **15**:338.
7. PUSEY, P. N. 1974. Macromolecular diffusion. *In* Photon Correlation and Light Beating Spectroscopy. Plenum Press, New York.
8. OSTER, G. 1948. The scattering of light and its applications to chemistry. *Chem. Rev.* **43**:319.
9. CUMMINS, H. Z., F. D. CARLSON, T. J. HERBERT, and G. WOODS. 1969. Translational and rotational diffusion constants of tobacco mosaic virus from Rayleigh linewidths. *Biophys. J.* **9**:518.
10. BORN, M., and L. WOLF. 1965. Principles of Optics. Pergamon Press, New York. Chapter 2.
11. PECORA, R. 1972. Laser light scattering from macromolecules. *Ann. Rev. Biophys. Bioeng.* **1**:257.
12. PECORA, R., and S. R. ARAGÓN. 1974. Theory of light scattering from hollow spheres. *Chem. Phys. Lipids.* **13**:1.
13. PUSEY, P. N., D. E. KOPPEL, D. W. SCHAEFER, R. D. CAMERINI-OTERO, and S. H. KOENIG. 1974. Intensity fluctuation spectroscopy of laser light scattered by solutions of spherical viruses: R17, Qβ, BSV, PM2 and T7. I. Light-scattering technique. *Biochemistry.* **13**:952.
14. BROWN, J. C., P. N. PUSEY, and R. DIETZ. 1975. Photon correlation study of polydisperse samples of polystyrene in cyclohexane. *J. Chem. Phys.* **62**:1136.
15. CHU, B. 1974. Laser Light Scattering. Academic Press, New York. Chapter VIII.
16. CHEN, F. C., W. TSCHARNUTER, D. SCHMIDT, and B. CHU. 1974. Measurement of diffusion coefficients of meningococcal polysaccharide by optical mixing spectroscopy. I. A preliminary characterization on the aggregation of the Group C polysaccharide. *Biopolymers.* **13**:2281.
17. CHU, B., A. YEH, F. C. CHEN, and B. WEINER. 1975. Self-association of β-lactoglobulin A in acid solution I. Translational diffusion coefficients. *Biopolymers.* **14**:93.
18. NISHIMURA, M., T. ITO, and B. CHANCE. 1962. A sensitive and rapid method of determination of photophosphorylation. *Biochim. Biophys. Acta.* **59**:177.
19. ARRIO, B., J. CHEVALLIER, M. JULLIEN, J. YON, and R. CALVAYRAC. 1974. Description by quasi elastic laser light scattering of a biological preparation: sarcoplasmic reticulum vesicles. *J. Membr. Biol.* **18**:95.
20. TANFORD, C. 1963. Physical Chemistry of Macromolecules. John Wiley & Sons, Inc., New York. Chapter 5.
21. TINKER, D. O. 1972. Light scattering by phospholipid dispersions: theory of light scattering by hollow spherical particles. *Chem. Phys. Lipids.* **8**:230.
22. PARADINE, C. G., and B. H. P. RIVETT. 1953. Statistics for Technologists. Van Nostrand-Reinhold, New York, Chapter XI.
23. MARTONOSI, A. 1964. Role on phospholipids in ATPase activity and Ca transport of fragmented sarcoplasmic reticulum. *Fed. Proc.* **23**:913.
24. REIF, F. 1965. Fundamentals of Statistical and Thermal Physics. McGraw-Hill, New York. Chapter 12.